X-ray Study of 2a. An orange prismatic crystal was mounted on a glass fiber. Data were collected at −72 °C on a Rigaku AFC6R diffractometer with graphite monochromated Mo Kα radiation (λ = 0.71069) and a 12 KW rotating anode generator. A total of 3590 reflections were collected of which 3367 were unique. Equivalent reflections were merged. The intensities of three representative reflections which were measured after every 197 reflections remained constant throughout data collection indicating crystal and electronic stability. No decay correction was applied. The structure was solved by a combination of the Patterson method and direct methods. The refinement was by full matrix least squares with TEXSAN. The *tert*-butyl group of the alkylidyne ligand failed to refine adequately as a full occupancy moiety. The disorder was modeled as a 2/1 orientation disorder with group isotropic temperature factors. The occupancy of the solvent was set at 0.50 because of the reasonable values of the refined temperature factors. The carbon of the solvent was refined isotropically. All other non-hydrogen atoms were refined anisotropically. Hydrogen atoms were included in calculated positions (d_{C-H} = 0.95 Å) (space group $P2_1/c$, a = 9.953 (4) Å, b = 12.398 (9) Å, c = 19.720 (6) Å, β = 93.08 (3)°, V = 2430 (2) Å^3, Z = 4, ρ = 1.473 g/cm^3, R = 0.050, R_w = 0.084). A full description of the structural study can be found in the supplementary material.

X-ray Study of 6a. Details of the structural study of **6a** can be found in Supplementary Material elsewhere.[8]

Acknowledgment. We thank the National Science Foundation for supporting this research (Grant CHE 88-22508) and for a predoctoral fellowship (to I.W.). We also thank the U.S. Department of Energy, Division of University and Industry Programs, for funds to purchase the X-ray diffractometer (Grant DE-FG05-86ER75292) and Dr. W. E. Crowe for useful discussions.

Supplementary Material Available: Complete NMR data for all compounds, description of the structural study of **2a** with an ORTEP drawing and a fully labeled drawing, and a listing of final positional and thermal parameters (18 pages); listing of final observed and calculated structure factors (22 pages). Ordering information is given on any current masthead page.

Singly Bridged Arrangements on Group 14 X_2H_4 Potential Surfaces

Georges Trinquier

Contribution from the Laboratoire de Physique Quantique, C.N.R.S. U.R.A. 505, Université Paul-Sabatier, 31062 Toulouse Cedex, France. *Received May 14, 1990*

Abstract: Theoretical exploration of the Sn_2H_4 and Pb_2H_4 singlet potential energy surfaces led to a local minimum corresponding to an isomer with an unsymmetrical structure presenting a single X-H-X bridge and a short X-X distance. For tin and lead, this isomer lies at 8 and 15 kcal/mol, respectively, above the preferred doubly bridged structure and at 25 and 13 kcal/mol, respectively, below the dissociation products $2XH_2(^1A_1)$. The molecule can be seen as two singlet XH_2 moieties bound by a three-center two-electron bridge and a $n_\sigma \rightarrow p_\pi$ dative bond $HX \leftarrow H \cdots XH_2$. Electronic correlation, analyzed through a CASCF+OVB procedure, strengthens the X-X bond and makes it more covalent, suggesting another limiting form $H\ddot{X}\text{-}XH_3$ with an internal H bridge. Several indexes support a direct Sn-Sn link stronger than that of Pb-Pb. These singly bridged forms occupy a key position on the group 14 X_2H_4 potential energy hypersurfaces since they can be topologically related to the doubly bridged forms (both trans C_{2h} and cis C_{2v}), the methylmethylene-like forms $H\ddot{X}\text{—}XH_3$ and the doubly bonded forms $H_2X{=}XH_2$. With germanium and silicon the singly bridged arrangement is caught in the well of $H\ddot{X}\text{-}XH_3$, but it should remain a crossing point between the four isomers. This provides a new global view of the X_2H_4 potential surfaces for which the largest number of true minima—five—is observed only for Sn_2H_4.

In a previous work, the existence of doubly bridged structures was established for group 14 X_2H_4 potential energy surfaces.[1] These geometries, which can be C_{2h} trans, **1**, or C_{2v} cis, **2**, have

1 **2**

proven to be true minima except for C_2H_4, where **1** was found to be a saddle point and **2** a critical point of index 2. The trans-bridged form **1** is even found to be the absolute minimum on the Sn_2H_4 and Pb_2H_4 surfaces. We report here the existence of another type of minimum corresponding to the singly bridged structure **3**. This unsymmetrical arrangement was found to be a true minimum on the Sn_2H_4 and Pb_2H_4 potential surfaces. Attempts to reach such a local minimum failed for the lighter analogues Ge_2H_4 and Si_2H_4, where the singly bridged arrangement is caught in the low hollow of the methylmethylene-type form $H_3X\text{-}XH$.

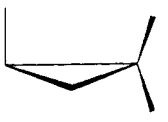

3

After a methodological section, we will comment on the structures of the singly bridged forms, trying to figure out a bonding scheme and to gauge correlation effects by use of orthogonal valence-bond (OVB) analyses. Then we will reconsider the shapes of the X_2H_4 potential hypersurfaces in relation to this new connecting point.

Computational Procedures

SCF calculations were performed with the PSHONDOG algorithm,[2a] which uses effective core potentials taking into account relativistic effects through mass correction and Darwin terms.[2b] The valence basis sets used are of double-ζ plus polarization (DZP) quality with polarization function exponents taken at $\eta_p(H)$ = 0.80, $\eta_d(Sn)$ = 0.20, and $\eta_n(Pb)$ = 0.15. Geometries were optimized with a gradient technique. The optimization is ended when the gradient components are lower than 10^{-4}. Harmonic force fields are calculated through a numerical derivation of the analytical first derivatives, using a single-point differencing formula. Correlation effects were not included in the optimization process since these were shown to have no dramatic influence on the geometries of the Sn_2H_4

(1) Trinquier, G. *J. Am. Chem. Soc.* **1990**, *112*, 2130.

(2) (a) Pélissier, M.; Komiha, N.; Daudey, J. P. *J. Comput. Chem.* **1988**, *9*, 298. (b) Barthelat, J. C.; Pélissier, M.; Durand, Ph. *Phys. Rev. A* **1981**, *21*, 1773.

0002-7863/91/1513-144$02.50/0

Table I. Optimized Geometrical Parameters, in Angstroms and Degrees[a]

	Sn_2H_4	Pb_2H_4
X_1X_2	2.744	2.936
X_1H_3	2.044	2.020
X_2H_3	1.915	2.133
X_1H_6	1.764	1.826
X_2H_4	1.723	1.786
X_2H_5	1.720	1.779
$H_3X_1X_2$	44.2	46.6
$H_3X_2X_1$	48.1	43.5
$X_1H_3X_2$	87.7	89.9
$H_6X_1H_3$	85.7	88.0
$H_4X_2H_5$	105.1	100.4
$H_6X_1X_2$	85.4	85.7
$X_1X_2H_4$	123.0	120.9
$X_1X_2H_5$	126.2	124.1
$H_6X_1X_2H_3$	88.6	91.3
$H_3X_1X_2H_4$	74.0	65.0
$H_3X_1X_2H_5$	75.5	66.1

[a] See Figure 1 for the definitions.

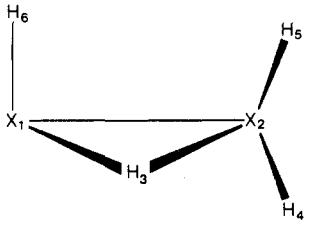

Figure 1. Atom labeling.

isomers.[3] Therefore, the correlated descriptions are made only for the SCF-optimized structures. Configuration interactions were performed with the CIPSI method.[4] The variational subspaces include all determinants that contribute to the first-order perturbed wavefunction by a coefficient larger than or equal to 0.02. This makes about 30 determinants in our systems. The MCSCF calculations were performed over a complete active space (CAS) of four electrons in five orbitals. For the singly bridged molecules, this makes 45 configurations, due to the lack of symmetry.

Structures and Bonding

1. SCF-Level Description. Structure **1** was first found by sliding down along the Pb_2H_4 potential surface, starting from the simple ethylenic planar form. Encountering two further saddle points, **4**, one finally reaches the unsymmetrical structure **3** exhibiting

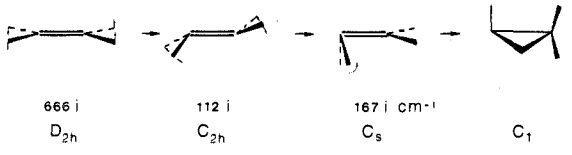

4

a typical Pb–H–Pb bridge and a rather short Pb–Pb bond length. Transferring this relative arrangement to the Sn_2H_4 surface led directly to the same kind of C_1 local minimum, while on the Ge_2H_4 and Si_2H_4 potential surfaces it slowly led to the germylgermylene form H_3Ge–GeH and to the silylsilylene form H_3Si–SiH.

The geometrical parameters for the singly bridged forms of Sn_2H_4 and Pb_2H_4 are listed in Table I (see Figure 1 for the definitions). The corresponding harmonic vibrational frequencies are listed in Table II. They are all real, which ensures that the C_1 singly bridged structures are true minima. The geometries are plotted in Figure 2. Both molecules are chiral and have similar shapes. The main differences between the tin and lead isomers concern (1) the $X_2H_4H_5$ group, which is more tilted out of the

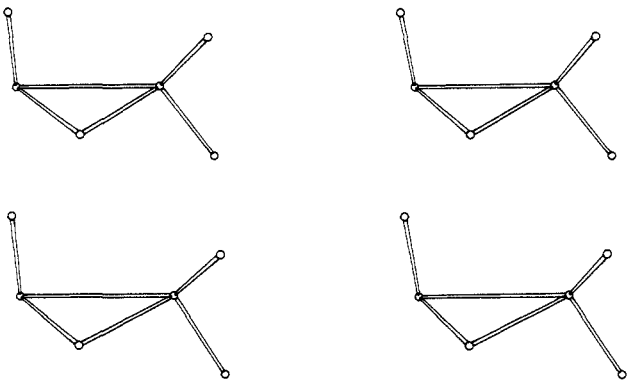

Figure 2. Stereodrawing of C_1 singly bridged forms for Sn_2H_4 (top) and Pb_2H_4 (bottom).

Table II. Harmonic Vibrational Frequencies (cm^{-1})

Sn_2H_4	Pb_2H_4	Sn_2H_4	Pb_2H_4	Sn_2H_4	Pb_2H_4
185	96	563	490	1387	1242
301	242	807	720	1895	1692
400	430	827	783	2015	1792
517	454	1003	855	2031	1805

Table III. SCF-Calculated Sn–Sn and Pb–Pb Bond Lengths (Å)

	Sn–Sn	Pb–Pb
H_3X—XH_3 (D_{3d})	2.80	2.84
H_2X=XH_2 (C_{2h})	2.71	3.00
HX—XH_3 (C_s)	2.89	2.96
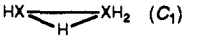 (C_1)	2.74	2.94
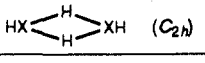 (C_{2h})	3.09	3.25

X_1X_2 direction in Pb_2H_4 than in Sn_2H_4 (see below Figure 5), and (2) the X_1–X_2 bond, shorter in Sn_2H_4 than in Pb_2H_4. The X–H bond lengths of the X_1–H_3–X_2 bridges are quite comparable to those in the doubly bridged structures (Sn–H 1.93 Å, Pb–H 2.04 Å). Since the valence angle at the bridging hydrogen is ~90°, the $X_1X_2H_3$ three-membered ring is almost a right-angled isosceles triangle. Note that in Sn_2H_4 the Sn_2–H_3 bond is shorter than the Sn_1–H_3 one, while it is the reverse for lead where the shorter bond is Pb_1–H_3. The X–X bonds are found to be rather short. Some typical X–X bond lengths calculated in similar conditions (SCF-DZP) are listed in Table III. The Pb–Pb bond in the singly bridged structure is shorter than that in HPb–PbH_3 but longer than the typical single bond calculated in H_3Pb–PbH_3. The Sn–Sn bond in the singly bridged structure is shorter than the typical single bond in H_3Sn–SnH_3. The $H_6X_1H_3$ moieties are quite similar to those in the C_{2h} doubly bridged structures. The $H_4X_2H_5$ moiety ressembles, through its bond lengths, the XH_3 group of HX–XH_3. Given the arrangement of the atoms and particularly the orientation of the $H_4X_2H_5$ group relative to $H_3X_1H_6$, the bonding in such an unusual structure may be viewed as two singlet methylene-like fragments—$X_1H_3H_6$ and $X_2H_4H_5$—bound through a three-center two-electron bridge X_1–H_3–X_2 and a dative bond n_σ (X_2) → p_π (X_1). In other words, the singlet $X_2H_4H_5$ fragment uses its empty p_π orbital on X_2 to build the hydrogen bridge with one X–H bond of its partner (X_1–H_3), while using its n_σ lone pair on X_2 to build a dative bond toward the p_π empty orbital of X_1, **5**. The n_σ lone pair on X_1, pointing outside the ring, keeps its

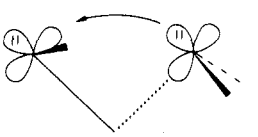

5

lone-pair character and does not contribute to the bonding. This bonding scheme is supported by the SCF wave functions. Can-

(3) Marquez, A.; Gonzalez, G. G.; Fernandez Sans, J. *Chem. Phys.* **1989**, *138*, 99.
(4) Huron, B.; Malrieu, J. P.; Rancurel, P. *J. Chem. Phys.* **1973**, *58*, 5745.

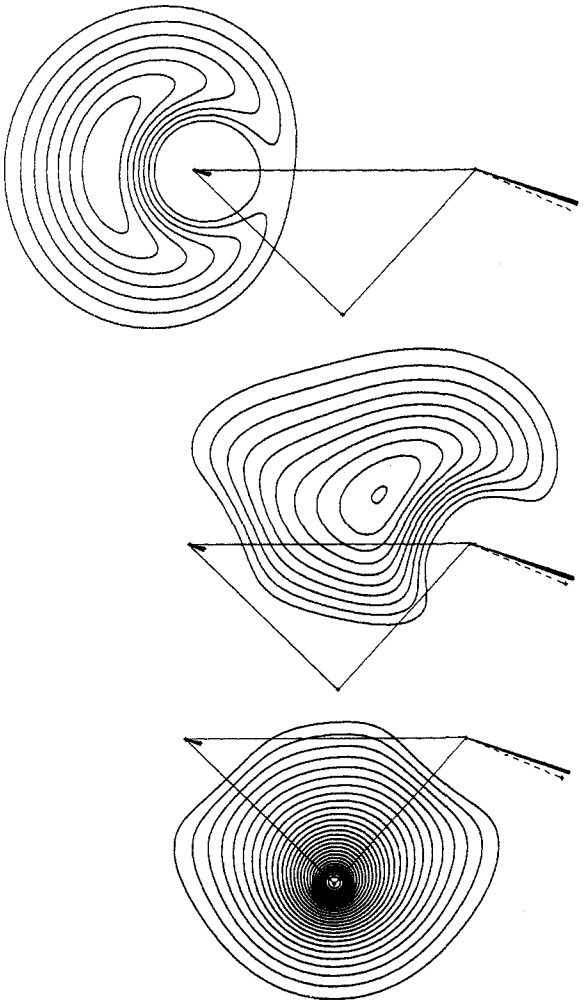

Figure 3. Occupied orbitals of C_1 Sn_2H_4 localized on the Sn–H–Sn bridge and on the Sn lone pairs. The curves are drawn in the Sn–H–Sn plane and correspond to values of Ψ starting from 0.100 and increasing by regular steps of 0.025.

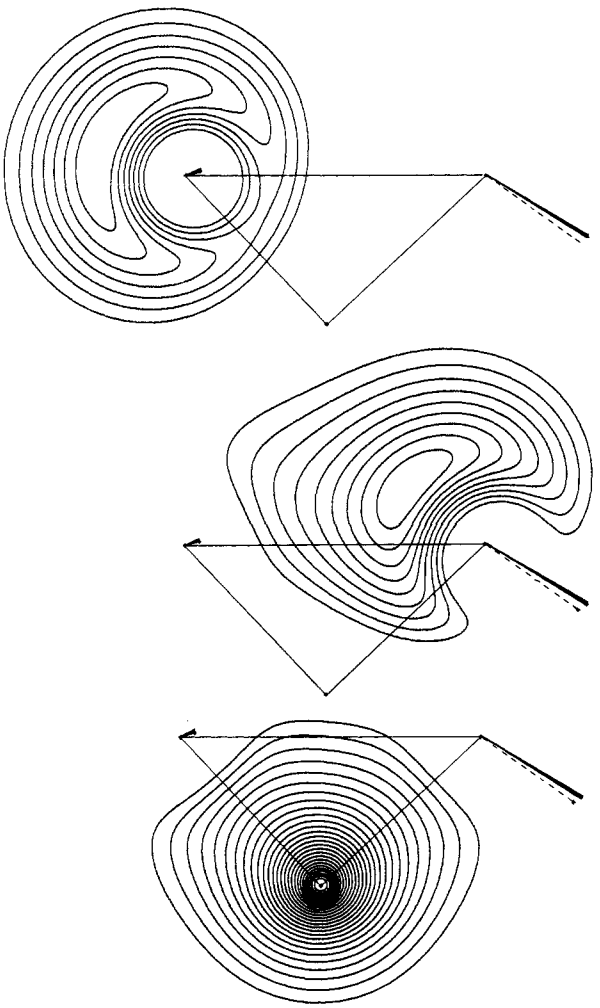

Figure 4. Occupied orbitals of C_1 Pb_2H_4 localized on the Pb–H–Pb bridge and on the Pb lone pairs. Same conventions as in Figure 3.

nonical delocalized orbitals include, both on Sn_2H_4 and Pb_2H_4, a regular and rather symmetrical orbital built on the $X_1H_3X_2$ bridge, and a set of two orbitals corresponding to the n_σ lone pairs. The one that is centered on X_2 actually takes significant components from X_1. Localizing the occupied orbitals according to Boys' criterion[5] makes their character even clearer. These are plotted in Figures 3 and 4, which show a bridge orbital essentially located on H_6, and two different n_σ lone pairs: that centered on X_1 is quite spherical and inert; that centered on X_2 is clearly deformed by the p component from X_1.

The geometrical parameters that do not involve the H_3 bridge atom recall the singlet $HX–XH_3$ structures. The similarity mainly concerns the bond lengths X_1H_6, X_2H_4, and X_2H_5 and the bond angle $H_6X_1X_2$. The Pb–Pb bond length in the singly bridged structure is also in line with that in $HPb–PbH_3$. The Sn–Sn bond length in the singly bridged structure is, however, unexpectedly short (see Table III). These similarities suggest another view of this C_1 structure, which may be derived from the $HX–XH_3$ isomer by rocking the XH_3 group to build an internal bridge, **6**. The

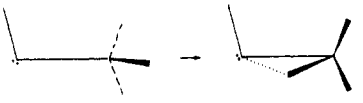

6

total electron density in the bridge plane, however, does not exhibit a high value along the X–X bonds, whereas the density is very strong on the X–H–X bridge, which has a strong ionic character (see Figure 5). Nevertheless, we must keep this scheme as a limiting form of the bonding. We shall see that correlation effects will actually restore much of the covalent character to the $n_\sigma \rightarrow p_\pi$ XX dative bond. Moreover, this limiting form happens to be more relevant for Sn_2H_4 than for Pb_2H_4. On the SCF geometries, this trend is seen from the X_1H_3 and X_2H_3 bond lengths and from the tilting of the $X_2H_4H_5$ groups, as previously mentioned. On the vibrational frequencies (see Table II) the lowest mode for the singly bridged structures corresponds to X–X stretching plus $H_3XH_4H_5$ rocking. It lies at 185 cm^{-1} in C_1 Sn_2H_4, which is in line with the Sn–Sn stretching frequency in $HSn–SnH_3$ (172 cm^{-1}). For Pb_2H_4, the two frequencies are further apart (96 cm^{-1} versus 122 cm^{-1}). Lastly, the Mulliken net charges listed in Table IV are closer to a $HSn–SnH_3$ scheme for Sn_2H_4 (in $HSn–SnH_3$ the net charges on the two tin atoms were calculated at +0.31 and +0.51, respectively) while they are closer to a diplumbylene scheme for Pb_2H_4 (in PbH_2 the net charge on lead was calculated at +0.41 while in $HPb–PbH_3$ the net charges on the two lead atoms were calculated at +0.36 and +0.34, respectively).

Table IV. Net Atomic Charges

	Sn_2H_4	Pb_2H_4
X_1	+0.36	+0.43
X_2	+0.48	+0.35
H_3	−0.26	−0.25
H_4	−0.19	−0.17
H_5	−0.18	−0.16
H_6	−0.21	−0.19
μ(D)	1.1	2.5

(5) Foster, J. M.; Boys, S. F. *Rev. Mod. Phys.* **1960**, *32*, 300.

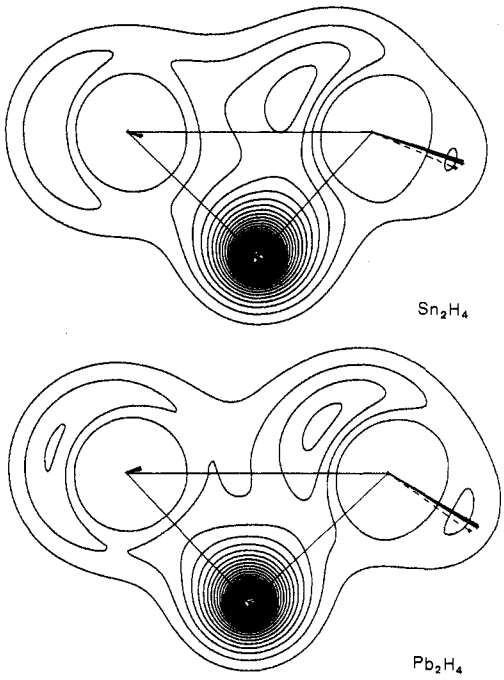

Figure 5. Valence total density in the $X_1H_3X_2$ plane for C_1 Sn_2H_4 and Pb_2H_4. The Ψ^2 curves start from 0.02 and increase by regular steps of 0.01.

2. Correlated-Level Description. Electronic correlation effects deserve to be examined in such a puzzling bond. To do so, MCSCF calculations were performed on both the doubly bridged and singly bridged structures.[6] The multiconfigurational expansion covers a complete active space (CAS) built on the proper combination of the orbitals involved in the bonding of the bridge or of the X–X link.

The active space underlying the binding in the singly bridged isomer consists of five orbitals, **7**, three of them being the classical

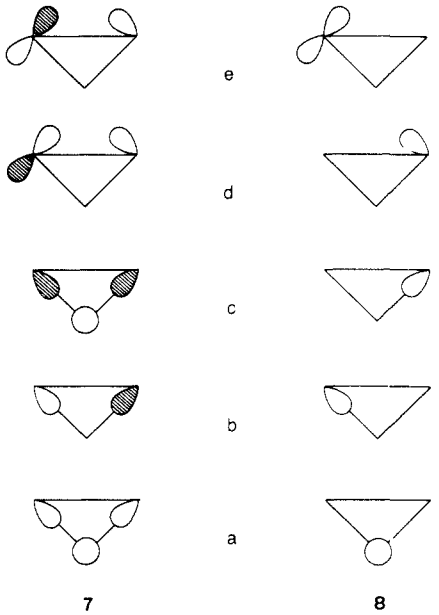

7 8

set of the three-center two-electron bond (**7a–c**), and the remaining ones being the bonding and antibonding n_σ/p_π combinations (**7d,e**). Orbitals labeled **7b**, **7c**, and **7e** are virtual orbitals, which are poorly characterized in the SCF wavefunction. In order to have a more reliable starting point for the CASSCF procedure, these three virtual orbitals were redefined according to a projection technique. The MCSCF calculations gave valence correlation energies of 20–30 kcal/mol for the various four-electron sets, with a coefficient of 0.98 for the fundamental determinant in all the multiconfigurational expansions. The details of these correlation energies are given in Table V. Selective configuration interactions from the CASSCF wavefunction were used to further decompose the correlation energy into intrapair and interpair contributions. Note in Table V that each X–H–X bridge contributes ~12 kcal/mol in a fairly constant way (this contribution was also calculated at 12.9 kcal/mol in the diborane prototype) while the n_σ pair on X_2 (or the X–X pair) only contributes one-half and one-third of this quantity in C_1 Sn_2H_4 and Pb_2H_4 respectively. The n_σ pair has therefore less bonding character. The interpair correlation between this n_σ X–X pair and the bridge in the C_1 isomers is larger than that between the two equivalent bridges in the C_{2h} isomers. In the doubly bridged compounds, valence-bond analyses support quite independent bridge bonds. Regarding the Sn/Pb difference, the correlation energy of the Sn–Sn pair is larger than that of the Pb–Pb pair, as expected from the rather short Sn–Sn distance.

Table V. Decomposition of the Correlation Energies of the Two Bonding Pairs in Doubly and Singly Bridged X_2H_4, As Calculated from CASSCF Procedures (kcal/mol)

		intrapair			
		X–H–X	n_σ	interpair	total
Sn_2H_4	C_{2h}	12.4		1.3	26.1
	C_1	12.0	6.4	3.7	22.1
Pb_2H_4	C_{2h}	13.0		1.2	27.2
	C_1	11.8	4.3	5.2	21.3

The MCSCF calculation localizes the five active orbitals on the $X_1X_2H_3$ three-membered-ring region. It is possible to further localize this set into five hybrids centered on the various atoms and pointing in the bonding directions, **8**. Since the XX/XHX separation is satisfactory in the canonical MCSCF orbitals, we have applied Boys' localization procedure[5] in each of the two subsets **7a–c** and **7d,e**. The hybrids obtained have enough local character to be used as a basis for the valence-bond decomposition of the CASSCF multiconfigurational wave function, as in classical OVB (orthogonal valence-bond) techniques. Our basis consists of $(C_5^2)^2=100$ VB determinants, which reduce to 45 space parts. As examples of such VB configurations, **9** and **10** are the neutral

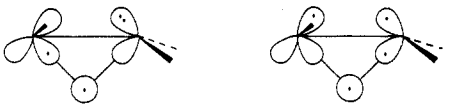

9 10

forms of the limiting Lewis arrangements mentioned earlier. These two VB forms are actually far from being dominant contributions, as can be seen in Table VI in which we have tried to summarize the results of the OVB analyses. First of all, neutrality is almost total within the two kinds of bonds since the ionic contributions corresponding to occupation of the two subsets by more than or less than two electrons is reduced to less than 1%. The next result shown in Table VI is the rather covalent character of the X–X bond. The correlated description gives a larger weight to the configurations that assign one electron to X_1 and one electron to X_2 rather than those that keep the pair on X_2. The bridge bond on X_1–H_3–X_2 mainly consists of an ionic form on H_3 and of the neutral forms. The contributions of the ionic forms on X_1 and X_2 are weak. The partition of the four electrons over the three atoms gives a net excess on X_2 (1.7 e^-).

The results given in Table VI suggest that for lead the singly bridged structure is closer to the diplumbylene adduct description, **5**, while for tin it is closer to the bridged-stannylstannylene description, **6**. For Sn_2H_4, the VB form **10**, associated with **6**, has a larger weight than that of **9**, associated with **5**. For Pb_2H_4, both

(6) The complete results concerning the doubly bridged systems in group 13 (X_2H_6) and group 14 (X_2H_4,$X_2H_6^{2+}$) will be published elsewhere (Trinquier, G.; Malrieu, J. P.; Garcia-Cuesta, I., manuscript in preparation). Only some results on doubly bridged Sn_2H_4 and Pb_2H_4 are given here for sake of comparison.

Table VI. Some Results of OVB Analysis of the $X_1X_2H_3$ Ring from MCSCF Wavefunctions (% Valence-Bond Forms)

	Sn_2H_4	Pb_2H_4
	8.2	15.3
	21.3	16.6
neutral 2 + 2 partition of the four electrons into the two subsets[a]	99.5	99.2
X_1—X_2 bond[b]		
	24.9	38.2
	63.1	55.0
	12.1	6.8
X_1—H_3—X_2 bond[b]		
	20.0	22.4
	27.6	34.3
	32.9	27.5
	12.6	9.9
	3.9	1.9
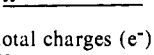	3.0	4.0
total charges (e^-)		
X_1	1.33	1.21
X_2	1.66	1.73
H_3	1.01	1.07

[a] The two subsets correspond to the two bonds X_1-X_2 (8d,e) and X_1-H_3-X_2 (8a–c). [b] For the neutral 2 + 2 partition of the four electrons, whatever the configuration of the two electrons in the remaining subset.

forms have about the same weight. For the X_1–X_2 bond, the relative proportion of the neutral form with respect to the ionic form on X_2 is larger in Sn_2H_4 (63/25) than in Pb_2H_4 (55/38). This trend is of course paralleled by the weight of the ionic form on X_1, which is stronger in Sn_2H_4 than in Pb_2H_4. On the bridge bond X_1–H_3–X_2, the forms that are neutral on H_3–X_2 have significantly larger weight than those that are neutral on X_1–H_3 in Sn_2H_4, while it is the reverse for Pb_2H_4. Moreover, although it is not easy to localize the electron pair of the bridge on the X atoms, it is easier to do so on X_2 in Sn_2H_4 and on X_1 in Pb_2H_4. This again suggests that the n_σ pair of the X–X bond is more retained on X_2 in the case of Pb.

Keeping in mind that these results strongly depend on (and reflect) the SCF geometries, with the short Sn–Sn distance, we will conclude that the bonding in the singly bridged systems can be understood through two limiting forms. Certain SCF geometrical parameters and the SCF wave functions favor an adduct between two singlet XH_2 dihydrides, with a three-center two-electron bridge and an $n_\sigma \rightarrow p_\pi$ dative bond. Other geometrical parameters, correlation effects, and OVB analyses favor a singlet methylmethylene-like structure HX–XH_3, distorted to allow a three-center two-electron bridge with one hydrogen of the XH_3 group. Overall, the results suggest that the C_1 isomer of Sn_2H_4 is closer to the methylmethylene-like structure.

Location on the Potential Surfaces

The relative energies of the unsymmetrical singly bridged forms with respect to their isomers are given in Table VII. The singly bridged form of Pb_2H_4 is halfway between the dissociation product $2PbH_2$ ($^1A_1$) and the C_{2h} doubly bridged absolute minimum. The binding energy of 13 kcal/mol with respect to two PbH_2 building blocks would support a regular hydrogen bridge plus a very weak direct Pb–Pb interaction. For Sn_2H_4, the singly bridged structure is only 8 kcal/mol above the preferred doubly bridged structure. It is bound by 25 kcal/mol with respect to $2SnH_2$ ($^1A_1$). This binding energy relative to the fragments supports a regular hydrogen bridge plus a rather strong Sn–Sn bond, which should contribute ~8 kcal/mol. These energetics are in line with the structural data regarding the Sn/Pb differences. Most interestingly, the C_1 isomer for Sn_2H_4 is close to the methylmethylene and trans-bent doubly bonded isomers. Our calculated energies locate the unsymmetrical singly bridged structure just in between HSn—SnH_3 and H_2Sn=SnH_2. On the Pb_2H_4 surface, the singly bridged structure is 2 kcal/mol below the C_{2h} H_2Pb=PbH_2 saddle point. Note therefore that these three minima are closer in energy for Sn_2H_4 than for Pb_2H_4.

Table VII. Calculated Relative Energies (kcal/mol)

	Sn		Pb	
	SCF	CI	SCF	CI
$2XH_2$ ($^1A_1$)	33.3	33.2	30.6	28.7
H_2X=XH_2 (C_{2h})	14.1	9.1	24.0[a]	23.9
H_3X—XH (C_s)	1.3	7.0	14.8	17.5
(C_1)	6.6	7.9	14.5	15.3
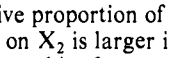 (C_{2v})	2.1	2.3	2.1	2.0
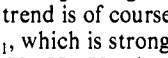 (C_{2h})	0	0	0	0

[a] Saddle point.

Grounding the topological links between the singly bridged form and its isomers both on the structural and energetic data, we can now picture the X_2H_4 potential surface. The unsymmetrical form occupies a key position on the surface since it can be connected to all its neighbors through slight geometrical changes, as shown in **11**. Simple rotation around H_3X_2 (3, 4) may lead to the doubly

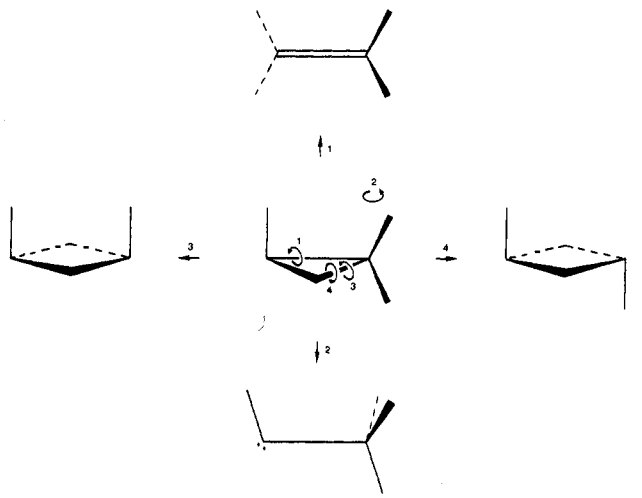

11

bridged structures without destroying the preexisting X_1–H_3–X_2 bridge. According to the way of rotation, the C_{2h} trans or the C_{2v} cis isomer are reached. The singly bridged structure is therefore expected to be the transition state during the cis–trans interconversion of the doubly bridged forms, **12**. Rotation around

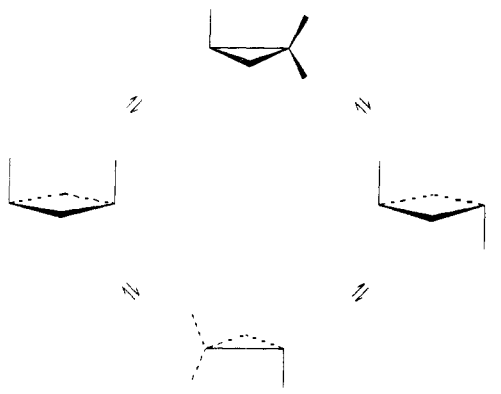

12

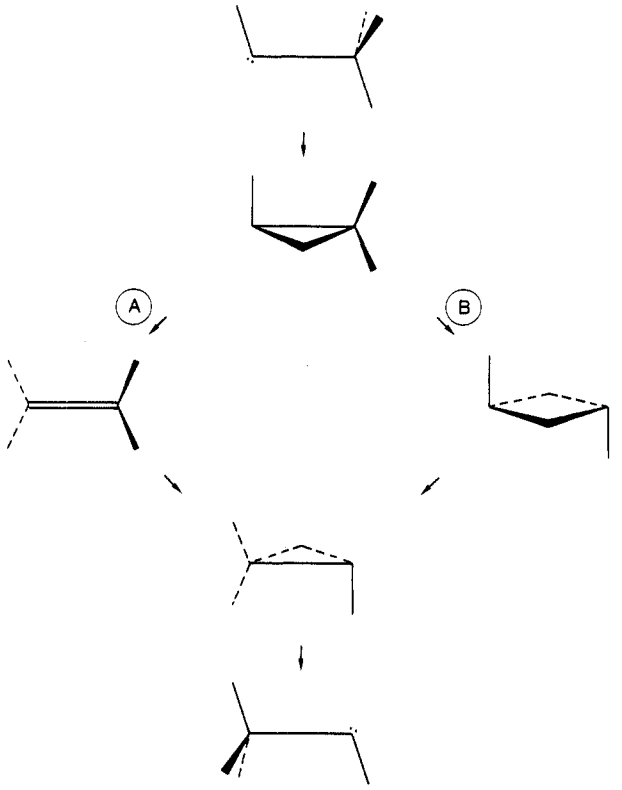

Figure 6. Connection of the singly bridged form with other stationary points.

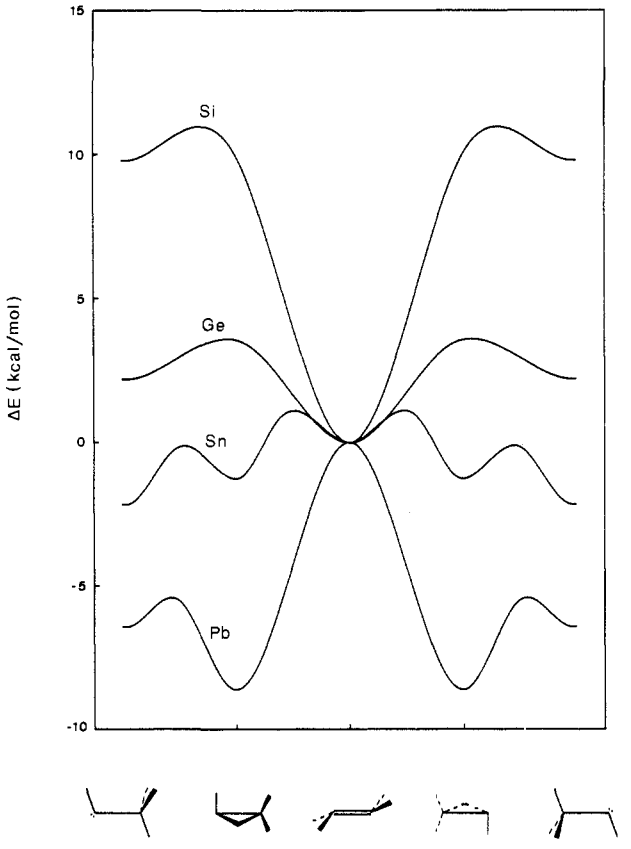

Figure 7. Schematic cross sections of the potential surfaces, along pathway A of Figure 6. The common zero energy corresponds to the doubly bonded isomers. Energy barriers are arbitrary.

X_1X_2 (1), destroying the H_3X_2 bridge, leads to the trans-bent doubly bonded isomer. Tilting the $H_3X_2H_4H_5$ group (2) destroys the H_3X_1 bridge and leads to the methylmethylene form. If we

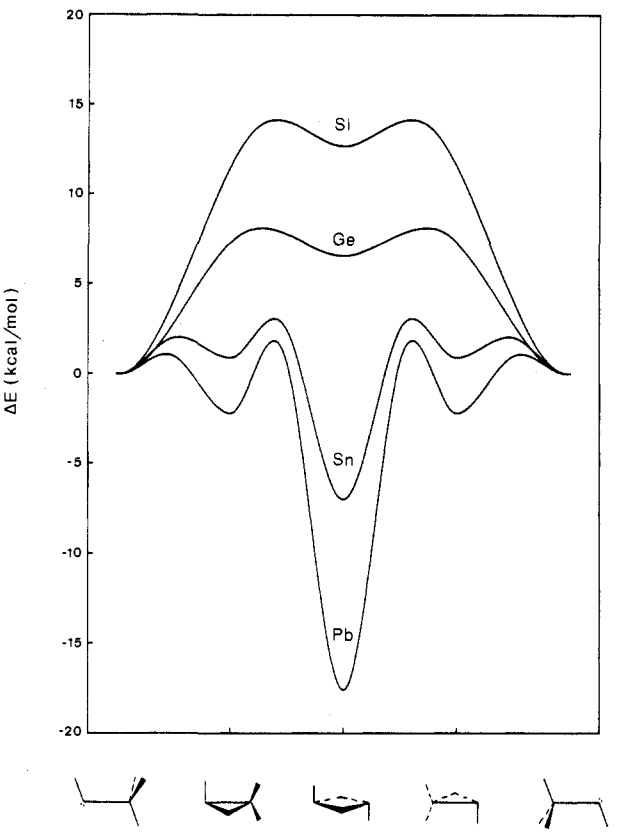

Figure 8. Schematic cross sections of the potential surfaces, along pathway B of Figure 6. The common zero energy corresponds to the methylmethylene-like isomers. Energy barriers are arbitrary.

try to represent the whole potential surface through a pathway connecting the two equivalent methylmethylene forms, **13**, as we

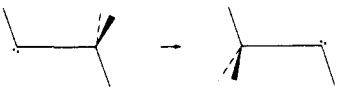

13

did in a previous work,[1] we must now take, as a key intermediate, the singly bridged structure, which is the bifurcation point for the two pathways, running through the doubly bonded structure or the doubly bridged structure, as schematized in Figure 6. The present scheme is more general and should supersede that proposed in Figure 2 of ref 1, which is incomplete regarding the new results.

In Figures 7 and 8, we have drawn the energy profiles corresponding to the two transits shown in Figure 6. The energy barriers are arbitrarily chosen and only serve to define the true minima. In Figure 7 (pathway A), the energy of the doubly bonded intermediate is placed at zero for clarity. Note that the higher the energy of the double-bonded structure with respect to that of $HX{-}XH_3$, the less stable the singly bridged intermediate. So, the disappearance of this minimum for the Ge_2H_4 and Si_2H_4 series satisfies a regular trend. More interesting is the pathway B, which runs through the doubly bridged intermediate (Figure 8). Here we have placed the methylmethylene-like forms at zero. Note on these curves that the deeper the doubly bridged minimum with respect to $HX{-}XH_3$, the deeper the singly bridged minimum. For Ge_2H_4 and Si_2H_4, the doubly bridged structure is higher in energy than the methylmethylene-like form. The disappearance of the singly bridged minimum therefore occurs due to its capture by the methylmethylene-like well, as seen for Ge_2H_4 and Si_2H_4. The present state of our routines does not enable us to locate the transition states and therefore the energy barriers in Figures 7 and 8. In order to estimate the barrier required to rearrange the singly bridged form into the trans doubly bridged form (rotation 4 in scheme **11**), a linear synchronous transit of 10 regular steps

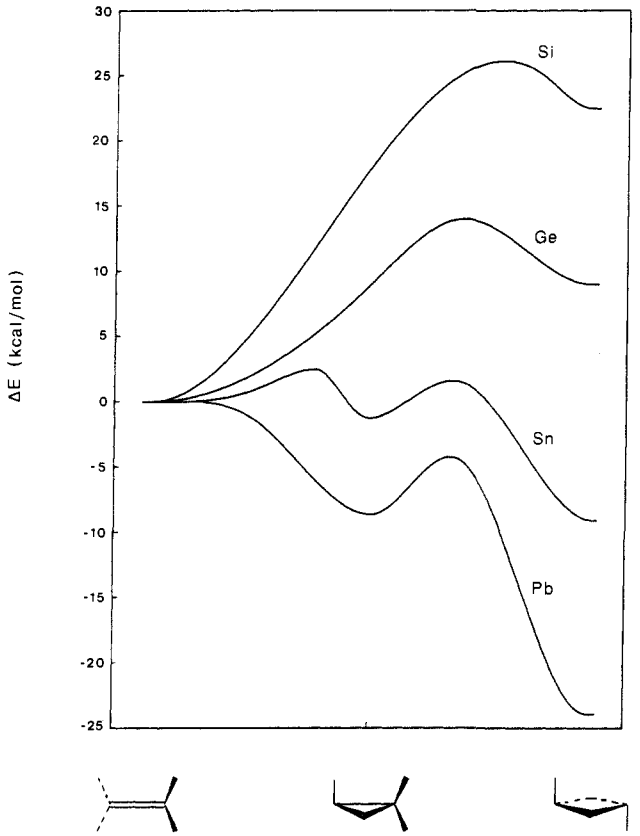

Figure 9. Schematic energy profiles linking the doubly bonded forms, the singly bridged forms, and the doubly bridged forms (pathway A + B of Figure 6). The common zero energy corresponds to the doubly bonded isomers. Energy barriers are arbitrary.

has been calculated between the two structures for Pb_2H_4. The transition state occurs at midpoint (fifth step), lying at 11.0 (SCF) and 12.8 kcal/mol (CI) above the singly bridged structure. This upper bound is certainly a poor estimate and we should only conclude in a barrier of 5–10 kcal/mol. Note that the barrier to overcome in the isomerization of the singly bridged structure into the C_{2v} cis doubly bridged structure, should be much weaker since there is less geometrical reorganization (see in **11** how rotation 3 is shorter than rotation 4). For tin and lead, energy profiles like **14** for the cis–trans interconversion cycles can

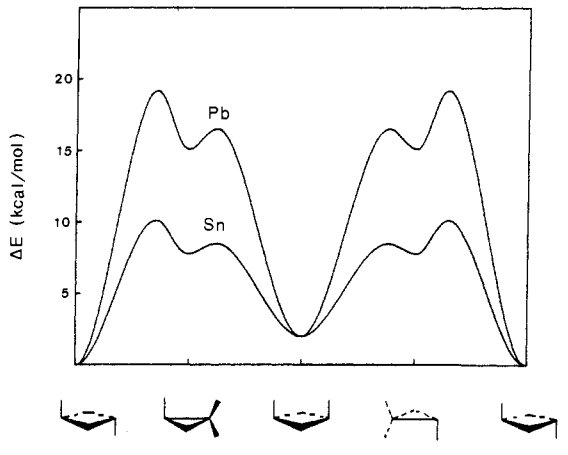

14

therefore be proposed. One could be tempted to draw curves for germanium and silicon that would be below that of tin and that would have a barrier corresponding to the singly bridged structure as saddle point. This would not be correct since for Ge_2H_4 and Si_2H_4 the singly bridged arrangements (in geometries extrapolated from those of C_1 Sn_2H_4 or Pb_2H_4) are calculated to lie below the trans doubly bridged structures. For Ge and Si indeed, the singly bridged geometries are in the catchment region of the $HX–XH_3$ form, which is lower in energy than the trans doubly bridged form (by 7 and 13 kcal/mol for Ge_2H_4 and Si_2H_4 respectively). Consequently, the cis–trans direct interconversion of the bridged forms of Si_2H_4 and Ge_2H_4 should not cross a barrier corresponding to a singly bridged form.

Although the C_1 singly bridged form is no longer a minimum on the Si_2H_4 and Ge_2H_4 potential energy surfaces, it may still be a connecting point linked to the doubly bonded, doubly bridged, and methylmethylene-like forms as schematized in Figure 6. For tin and lead, the C_1 form is an intermediate step during the double-bond/double-bridge interconversion. Again, it cannot be a saddle point for silicon or germanium since in these cases it is located below the doubly bridged isomer. The energy profiles for these isomerization paths are plotted in Figure 9, which further shows that the singly bridged minimum only exists when the doubly bridged isomer is lower than the doubly bonded isomer.

On the Si_2H_4 and Ge_2H_4 potential energy surfaces, the singly bridged structures are in the catchment region of the methylmethylene-type forms $H\ddot{X}–XH_3$. A simple explanation for the disappearance of the singly bridged minimum on these surfaces is the deepness of the $HX–XH_3$ minimum located below the C_{2h} doubly bridged minimum (at −7 kcal/mol for Ge_2H_4 and −13 kcal/mol for Si_2H_4). For Sn_2H_4 and Pb_2H_4 the $HX–XH_3$ minimum is located above the C_{2h} doubly bridged minimum (at +7 and +17 kcal/mol, respectively). It can be conceived that the lowering of the $HX–XH_3$ minimum from +7 (Sn) to −7 kcal/mol (Ge) destroys the intermediate singly bridged minimum. To illustrate this, let us draw a two-dimensional map with two coordinates corresponding to rotation 1 (or 2) in **11** for the horizontal axis and to the conversion singly bridged → methylmethylene (mainly, but arbitrarily, tilting 2 in **11**) for the vertical axis. On such a map, there are four minima for Pb_2H_4 and Sn_2H_4, **15**.

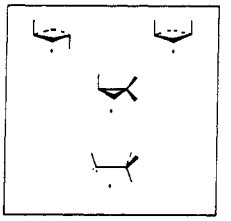

15

Why the singly bridged minimum is caught by the $HX–XH_3$ minimum follows from that property of potential energy surfaces according to which a prominent change in the relative heights of two minima may change the nature of other stationary points.[7-10] The phenomenon is schematized on the maps of Sn_2H_4, **16**, and Ge_2H_4, **17**.

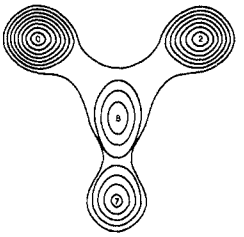

16

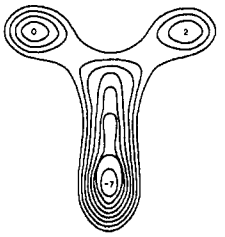

17

(7) Csizmadia, I. G. In *New Theoretical Concepts for Understanding Organic Reactions*; Bertran, J., Csizmadia, I. G., Eds.; Kluwer Publications: Dordrecht, The Netherlands, 1989; p 1.

(8) Mezey, P. G. In *New Theoretical Concepts for Understanding Organic Reactions*; Bertran, J., Csizmadia, I. G., Eds.; Kluwer Publications: Dordrecht, The Netherlands, 1989; p 55, 77.

(9) Mezey, P. G. *Potential Energy Hypersurfaces*; Elsevier: Amsterdam, 1987.

(10) Iratçabal, P.; Liotard, D. *J. Am. Chem. Soc.* **1988**, *110*, 4919.

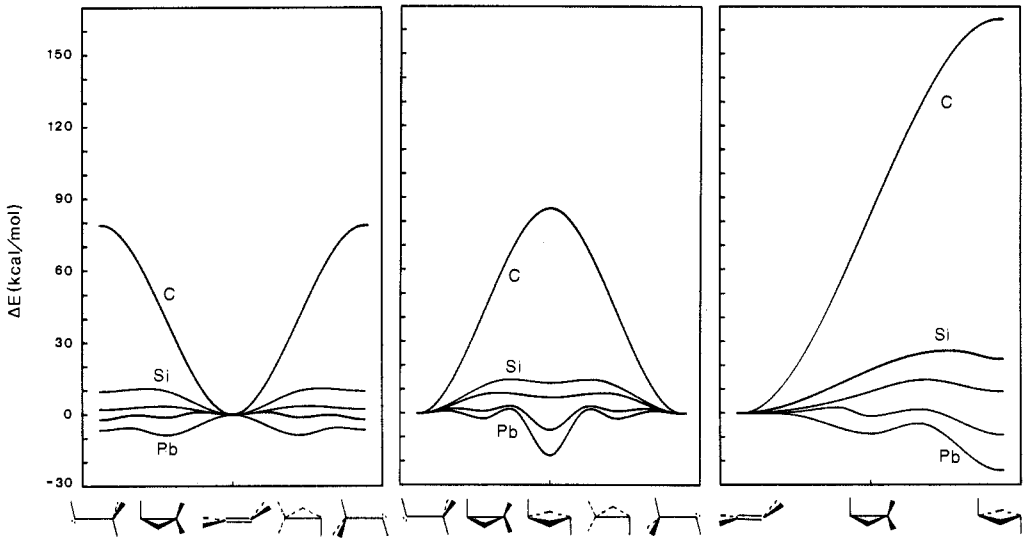

Figure 10. Same as Figures 7–9, on another scale, and including the carbon series.

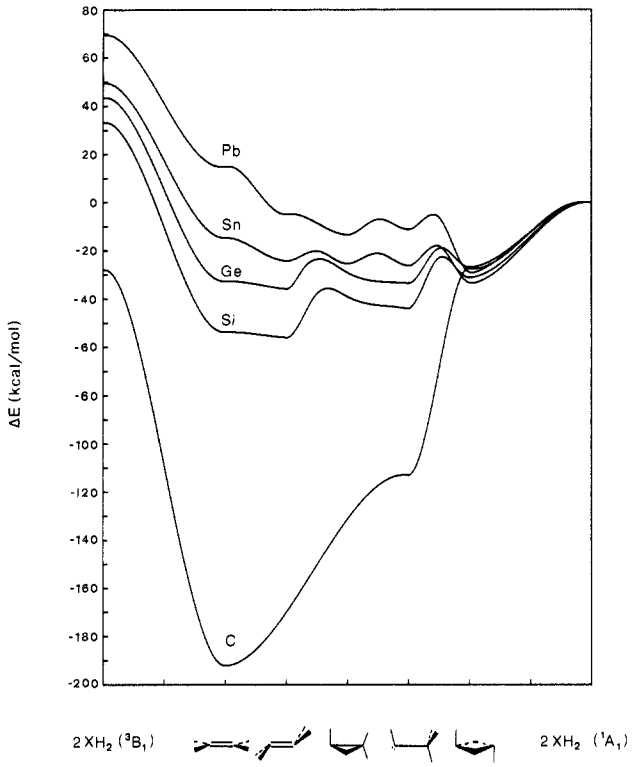

Figure 11. Schematic view of the group 14 singlet X_2H_4 potential energy surfaces, connecting from left to right: $2XH_2$ ($^3B_1$), the planar double bond, the trans-bent double bond, the singly bridged structure, the methylmethylene-like structure, the trans doubly bridged structure, and $2XH_2$ ($^1A_1$), which is the zero energy common to all surfaces. The coordinate on the horizontal axis and the energy barriers are arbitrary.

If we now include the carbon series in our hypersurface cross sections, we shall have an idea of the whole of the group 14 X_2H_4 potential energy surfaces. This is done in Figure 10. As usual, the potential curves relative to C_2H_4 are singular inasmuch as there is a very stable structure, the planar π-bonded form, corresponding to a single well. The other structures' methylmethylene and bridged forms are very high in energy and are not true minima (singlet methylmethylene is found to be a true minimum at the SCF level but further treatments would probably change the nature of this stationary point).[11]

(11) Hehre, W. J.; Radom, L.; Schleyer, P. v. R.; Pople, J. A. *Ab Initio Molecular Orbital Theory*; John Wiley and Sons: New York, 1986; p 426.

Discussion and Conclusion

The problem of the group 14 X_2H_4 hypersurfaces may be summarized as follows. For carbon, there is a single minimum—the deep well corresponding to the stable π-bonded form $H_2C{=}CH_2$. Going down to heavier elements, the doubly bonded form remains a minimum (although it becomes trans-bent distorted) except for Pb_2H_4, where simple modeling predicts that it no longer exists. Beyond carbon, two other minima appear, corresponding to the carbene-like form $H\ddot{X}\text{-}XH_3$ and the doubly bridged form $HX{<}^{H}_{H}{>}XH$ (with two possible arrangements, cis C_{2v} and trans C_{2h}, nearly degenerate in energy). Beyond germanium, for Sn_2H_4 and Pb_2H_4 a fourth type of minimum appears, corresponding to the unsymmetrical singly bridged structure with an X–X bond. The total number of possible minima is therefore five: (1) double bond (planar or trans-bent), (2) methylmethylene-like form, (3) trans double bridge, (4) cis double bridge, and (5) single bridge. The five minima all exist only on the Sn_2H_4 potential surface, where they happen to be rather close in energy (within 10 kcal/mol; see Table VII). Moving to the other group 14 elements privileges one or another form of unsaturation, resulting in the disappearance of some minima. For Pb_2H_4, the five possible arrangements are within 24 kcal/mol and the preferrence for bridged structures comes with the vanishing of the doubly bonded structure. For germanium and silicon, the minima are within 12 and 25 kcal/mol, respectively. The primacy of the carbene-like forms over the doubly bridged froms induces the vanishing of the singly bridged forms. For carbon, the very great stability of the $\sigma + \pi$ C=C bond prevents the existence of the other minima, which would be very high in energy and only are at most saddle points.

In Figure 11 we have pictured the shape of the whole potential surfaces for the X_2H_4 isomers and their dissociation products $2XH_2$. In this scheme, the separated singlet fragments $2XH_2$ ($^1A_1$) are taken as the common zero energy (right-hand-side asymptote) while the triplet fragments $2XH_2$ ($^3B_1$) are connected to their direct coupling product, namely, planar $H_2X{=}XH_2$. This figure, which replaces and completes Figure 4 of ref 1, shows the large gap between carbon and the heavier elements. For carbon, there is virtually a single deep trench. Beyond this element, other minima are created on the potential surfaces. Finally, the surface that has the largest set of true minima is that of Sn_2H_4 in which all the minima are within a rather narrow energy range.

Acknowledgment. The author is grateful to Dr. J.-P. Malrieu for his interest in this work and for valuable suggestions. He also thanks Drs. J.-P. Daudey and D. Liotard for helpful discussions, Dr. F. Spiegelmann for computational advices, and P. Lecante for assistance in the stereodrawing.